ELSEVIER

International Journal of Heat and Fluid Flow 22 (2001) 460–472

International Journal of HEAT AND FLUID FLOW

www.elsevier.com/locate/ijhff

Laminar flow and heat transfer through square duct with twisted tape insert

S. Ray [a,*], A.W. Date [b]

[a] *Department of Mechanical Engineering, Jadavpur University, Calcutta 700 032, India*
[b] *Department of Mechanical Engineering, Indian Institute of Technology, Bombay, Powai, Mumbai 400 076, India*

Received 15 June 1999; accepted 22 February 2000

Abstract

Numerically predicted characteristics of laminar flow and heat transfer through square duct with twisted tape insert are presented in this paper. The transport equations are solved on a non-staggered non-orthogonal grid using the curvilinear version of the "Complete Pressure Correction" algorithm. Both the flow and heat transfer are in a state of periodic development in the axial direction. The heat transfer characteristics are predicted under axially and peripherally constant wall heat flux conditions. Correlations for friction factor and Nusselt number are developed from the predicted data. The agreement between the correlation and experimental data for friction factor is found to be excellent. Relative thermo-hydraulic performance of square and circular ducts, both fitted with twisted tapes of same twist ratio is also presented in this paper. The study shows significant improvements can be achieved with the square duct, particularly at higher Prandtl numbers and lower twist ratios. Improvement is observed even for air, over certain ranges of Reynolds number. © 2001 Published by Elsevier Science Inc.

Keywords: Numerical; Laminar; Square duct; Twisted tape; Thermo-hydraulic performance

1. Introduction

Heat transfer augmentation techniques find applications mainly in the design of more compact heat exchanges. Various industries, especially the refrigeration, automotive and chemical process industries are becoming strong users of this technology. As a result, the technology of enhanced heat transfer has received serious attention over last 30–35 years. Due to its industrial importance, a large number of research publications as well as excellent review articles (Bergles, 1969, 1973, 1981a, 1985; Bergles and Joshi, 1983; Webb, 1987) are available in this area. Among the various augmentation techniques, the use of twisted tape inserts is an effective method to improve the thermo-hydraulic performance of laminar flow heat exchangers, since it offers significant increase in heat transfer as compared to the pressure drop, particularly at high Prandtl numbers (Manglik and Bergles, 1993a,b).

Almost all of the reported studies on twisted tapes have dealt with the flow through a circular duct. However, in many engineering applications, a square duct geometry is encountered (for example, plate fin heat exchangers). We are aware of only two works of Mano et al. (1986) and Bhadsavle (1994), where few experimental results are provided for flow through a square duct with twisted tape inserts. Both of these studies provided empirical correlations for friction factor, which not only differ in their form, but also show little agreement with each other (Ray, 1999). Compared to a circular tube, the square duct provides higher surface area to volume ratio, although its corners normally act as ineffective heat transfer surfaces (hot spots) as compared to the straight portions. Since, the twisted tape generates secondary circulation (which provides some scavenging effect), it is therefore worth while to study the performance of twisted tape generated swirl flow through a square duct.

In a heat transfer augmentation technique, the enhancement is brought about mainly by reducing the thermal boundary layer thickness. This reduction, in turn, is brought about by inducing force fields of various kinds or by disruption in the growth of viscous sublayers. Most typically, however, heat transfer enhancement is accompanied by increase in pressure drop and hence, pumping power. As such, while introducing enhancement techniques, care must be taken to ensure that overall thermo-hydraulic performance is superior to that of the basic duct geometry.

The purpose of the present paper is therefore, two folds: (i) to provide reliable correlations for both friction factor and Nusselt number and (ii) to study the relative thermo-hydraulic performances of square and circular ducts.

The geometry of the present problem is shown in Fig. 1. It consists of a square duct with cross-sectional area $a \times a$ and a tape fitted inside the duct. The tape has a pitch "H" for 180° rotation. The cross-section of the duct, at a twist

* Corresponding author.
E-mail address: subho@juphys.ernet.in (S. Ray).

0142-727X/01/$ - see front matter © 2001 Published by Elsevier Science Inc.
PII: S0142-727X(01)00078-9

Notation

a	side of the square duct, m
A	cross-sectional area, m^2
B	body force
C_p	specific heat at constant pressure, J/kg K
dA_i	area, perpendicular to ξ_i coordinate surface
D	diameter of the circular duct, m
D_i	general diffusion coefficient
f	friction factor
J	Jacobian of the coordinate transformation
H	pitch of the twisted tape for 180° rotation,
h	heat transfer coefficient, W/m^2 K
h_{x3}	local heat transfer coefficient, W/m^2 K
$\bar{h}$	pitch-averaged heat transfer coefficient, W/m^2 K
p	pressure, N/m^2
k	thermal conductivity, W/m K
L	length of the tube, m
$\dot{m}$	mass flow rate, kg/s
Nu	Nusselt number
Nu_{x3}	local Nusselt number
$\overline{Nu}$	pitch-averaged Nusselt number
P	modified pressure N/m^2
Pr	Prandtl number
q_i^ϕ	flux of scalar ϕ in the i direction
q_w	wall heat flux, W/m^2
$\dot{Q}$	rate of heat transfer, W
R_i	performance evaluation criterion ($i = 1, 7$)
Re	Reynolds number
S_ϕ	source term in the ϕ conservation equation
Sw	swirl parameter
T	temperature, K
T_b	bulk temperature, K
$\bar{T}_w$	average wall temperature, K
u_i	Cartesian velocity component ($i = 1, 2, 3$), m/s
$\bar{u}_3$	average axial velocity m/s
U_i	contravariant velocity component ($i = 1, 2, 3$), m/s
x_i	Cartesian coordinates ($i = 1, 2, 3$), m
Y	twist ratio ($= H/a$)

Greeks

β_i^j	geometrical factor ($i = 1, 2, 3,\ j = 1, 2, 3$)
β_p	average axial pressure drop, N/m^3
δ	tape thickness, m
ΔT_3	temperature rise over length of the computation domain, K
Γ^ϕ	effective diffusivity for scalar ϕ, kg/m s
ϕ	general variable
μ	dynamic viscosity, N s/m^2
θ	twist angle, degrees
ρ	density, kg/m^3
σ	turbulent Prandtl number
τ_{ij}	stresses ($i = 1, 2, 3,\ j = 1, 2, 3$), N/m^2
ξ_i	curvilinear coordinates ($i = 1, 2, 3$), m

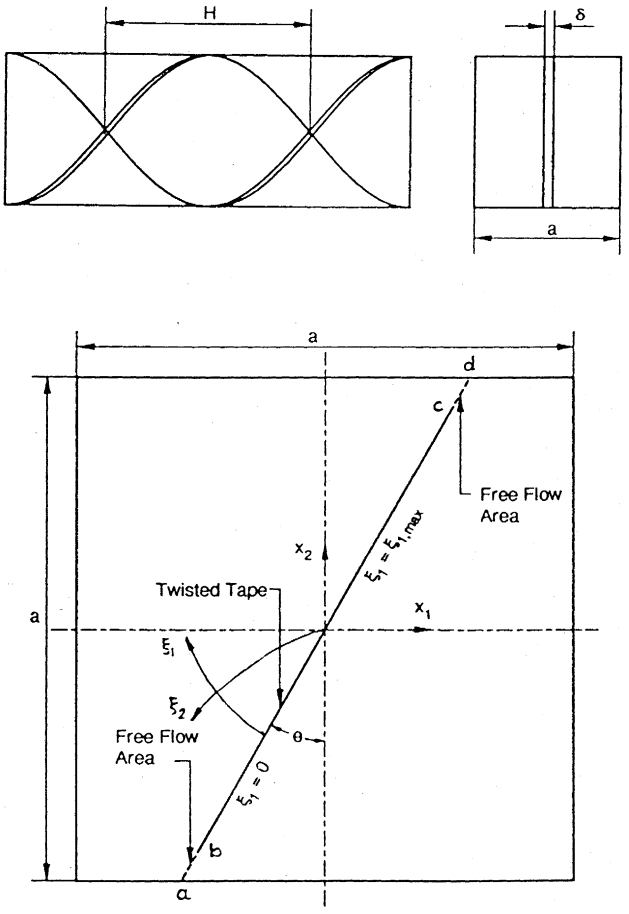

Fig. 1. Geometry of the square duct with twisted tape insert.

angle θ, is presented in Fig. 1(b), that for $\theta = 0$ can be seen in Fig. 1(a).

When a twisted tape is inserted in a square duct, the tape makes contact with the duct surface after each 90° rotation (or, at cross-sections $H/2$ apart). For any other twist angle (θ), the tape loses contact with the duct surface and the fluid is allowed to move from one half to another. Thus, the flow becomes periodically fully developed in the axial direction. It may also be noted that at any cross-section, the flow will exhibit cross-mirror-image symmetry about the tape surface. Hence, the analysis may be performed on a cross-section on any one side of the tape. Although the area of such a cross-section will remain constant, its shape and orientation will be repeated only after every $2H$ distance along the axial direction. For a forced convection situation, when half of the duct cross-section is considered for analysis (as in the present case), the flow at each cross-section in the free flow area ("ab" and "cd" in Fig. 1(b)) is also periodic, as the exit condition of the fluid in one half becomes identical with the entry condition for the other half and vice versa. This periodicity is called the "cross periodicity".

In Section 2, the mathematical formulation is presented. The computational aspects are briefly discussed in Section 3. The results for laminar flow and heat transfer are presented in Section 4. Section 5 presents the study on relative thermo-hydraulic performances of ducts of square and circular cross-sections and the conclusions are reported in Section 6.

2. Mathematical formulation

2.1. Governing equations

In the present analysis, the fluid properties are assumed to be uniform. The general form of the governing conservation equations for laminar flow of an incompressible fluid with

negligible viscous dissipation and buoyancy effects can be written in generalised curvilinear coordinates as follows,

$$J\frac{\partial}{\partial t}(\rho\phi)+\sum_{i=1}^{3}\frac{\partial}{\partial\xi_i}\left[\rho U_i\phi-D_i\frac{\partial\phi}{\partial\xi_i}\right]=S_\phi, \tag{1}$$

where D_i and S_ϕ are interpreted in Table 1. Further definitions are given in Table 2. The tables show that when $\phi=1$, mass conservation equation is retrieved. The momentum equations are written for Cartesian velocity components ($\phi=u_j$). It is important to note that the term $D_i\partial\phi/\partial\xi_i$ represents the dummy diffusion normal to $\xi_i=$Constant surfaces. The true Cartesian diffusion is included in the source terms through gradients of stresses, τ_{ij}, and scalar fluxes q_k^ϕ.

Patankar et al. (1977) have suggested that for a periodically fully developed flow, the pressure at any point can be split into two parts as follows,

$$p(x_1,x_2,x_3)=-\beta_{\mathrm{p}}x_3+P(x_1,x_2,x_3). \tag{2}$$

In the above equation, $\beta_{\mathrm{p}}(=\Delta\bar{p}/2H)$ is the mean axial pressure gradient over a distance $2H$ in the axial direction. Substitution of Eq. (2) in the momentum equations yields new sets of equations. The form of the x_1 and x_2 momentum equations remains same as Eq. (1). In all the momentum equations, p is replaced by the newly defined pressure, P. The x_3 momentum equation now contains an additional source term, $J\beta_{\mathrm{p}}$.

2.2. Boundary conditions

In the present method, the solutions are obtained only for the interior points. This is done by eliminating the boundary points from the discretised equations for near boundary control volume, using the boundary conditions. The boundary values are estimated subsequently from the solutions of the interior points. For further details, see Ray (1999). The boundary conditions for the present problem can be classified into two categories:

1. Wall condition,
2. Periodicity condition.

2.2.1. On the solid surfaces

On the duct and the tape surfaces, all the velocities are set equal to zero to implement the no-slip condition. The duct is also subjected to a constant axial and peripheral wall heat flux. Therefore, the boundary conditions can be expressed as

$$u_j=0,\quad \text{for } j=1,2,3,\quad \text{and} \tag{3}$$

$$-k\partial T/\partial n=q_{\mathrm{w}}\quad \text{at } \xi_2=\xi_{2,\max}, \tag{4}$$

where "n" denotes the normal derivative and q_{w} represents the applied wall heat flux. Therefore, $q_w=0$, on the tape surface as the tape is considered to be insulated.

2.2.2. Axial periodicity

The axial periodicity condition at the inlet (i.e., $x_3=0$ or $\xi_3=0$) and the exit (i.e., $x_3=2H$ or $\xi_3=\xi_{3,\max}$) of the computational domain are represented by

$$\begin{aligned}&u_j\,|_{\xi_3=0}=u_j\,|_{\xi_3=\xi_{3,\max}}\quad \text{for } j=1,2,3,\\ &P\,|_{\xi_3=0}=P\,|_{\xi_3=\xi_{3,\max}},\\ &T\,|_{\xi_3=0}+\Delta T_3=T\,|_{\xi_3=\xi_{3,\max}},\end{aligned} \tag{5}$$

where ΔT_3 is the bulk temperature rise over $2H$ axial distance, which is evaluated from the overall heat balance for a specified q_{w}.

2.2.3. Cross-periodicity

The cross-periodicity condition in the fluid domain (free flow area) for the half duct, at any axial station, can be represented as

$$u_{1,2}\,|_{\xi_1=0}=-u_{1,2}\,|_{\xi_1=\xi_{1,\max}},\quad u_3,T,P\,|_{\xi_1=0}=u_3,T,P\,|_{\xi_1=\xi_{1,\max}}. \tag{6}$$

2.3. Grid generation

Since the shape of the duct cross-section continuously changes along the axial direction, the physical computational domain is mapped into a transformed plane. However, instead of generating three dimensional grid in the whole computational domain, a two dimensional mapping is used at different axial locations. Therefore, at a particular cross-section (axial plane) the value of the x_3 coordinate remains same. When the corresponding nodes at each cross-section are connected, a three dimensional nonorthogonal grid is formed, spanning the entire domain of computation. In the present study, an elliptic grid

Table 1
Meaning of D_i and S_ϕ

ϕ	D_i	S_ϕ
1	0	0
u_j	$\mu dA_i^2/J$	$-\sum_{k=1}^{3}\beta_k^j\partial p/\partial\xi_k$ $+\sum_{i=1}^{3}\partial\left[\sum_{k=1}^{3}\beta_i^k\tau_{jk}-D_i\partial u_j/\partial\xi_i\right]/\partial\xi_i$ $+B_j$.
T	$\Gamma^T dA_i^2/J$	$-\sum_{i=1}^{3}\partial\left[\sum_{k=1}^{3}\beta_i^k q_k^T+D_i\partial T/\partial\xi_i\right]/\partial\xi_i$

Table 2
Terms in Table 1

Symbol	Meaning	Definition
U_i	Contravariant flow velocity	$\sum_{j=1}^{2}\beta_i^j u_j$
τ_{ij}	Stresses	$(\mu/J)\sum_{k=1}^{3}(\beta_i^k\partial u_j/\partial\xi_k+\beta_k^j\partial u_i/\partial\xi_k)$
q_k^ϕ	Flux of ϕ	$-(\Gamma^\phi/J)\sum_{j=1}^{3}\beta_j^k\partial\phi/\partial\xi_j$
Γ^ϕ	Diffusivity of ϕ	(μ/Pr)
β_j^i	Geometric coefficients	$(\partial x_j/\partial\xi_k)(\partial x_k/\partial\xi_i)-(\partial x_j/\partial\xi_i)(\partial x_k/\partial\xi_k),\ k\neq i,j$
J	Cell volume	$\sum_{k=1}^{3}\beta_i^k\partial x_k/\partial\xi_i,\quad i=1,2$ or 3
dA_i	Cell-face area	$\left[\sum_{j=1}^{3}(\beta_i^j)^2\right]^{1/2}$
B_j	Body force	

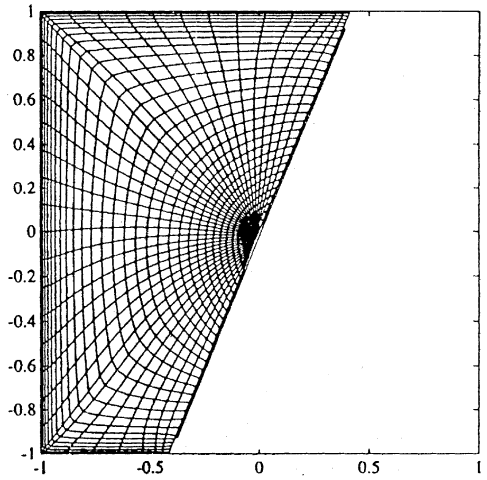

Fig. 2. Typical numerical grid for $\theta = 22.5°$.

generation technique, suggested by Sorenson (1980), is adopted to construct the grids at different cross-sections of the duct.

First, the computations are carried out on a 15 (in ξ_1) $\times$ 10 (in ξ_2) $\times$ 13 (in ξ_3, for $2H$ periodicity) nonuniform grid, for high Reynolds number ($Re \simeq 1100$) and Prandtl number ($Pr = 500$). Subsequently, the grid is refined to $23 \times 18 \times 25$. Final computations were carried out on a $39 \times 32 \times 49$ grid as with the further refinement of grid to $67 \times 62 \times 89$ the variation in f, Re and $\overline{Nu}$ were observed to be within 0.5%. This provides $37 \times 30 \times 47$ control volumes in the computation domain. At $\xi = 0$ and $\xi_1 = \xi_{1,\max}$, while specifying the boundary node distribution, special care is taken, such that one of the cell faces is aligned with the tip of the tape. At these locations, 25 cell boundaries are considered on the tape surface and the rest are provided in the fluid domain (free flow area). Typical grid chosen for $\theta = 22.5°$ is presented in Fig. 2.

3. Computational details

3.1. Method of solution

The transport equations, as given in Eq. (1), are discretised by a control volume based finite difference method, with power law approximation for the convective terms, on a nonstaggered grid. The solutions of the discrete equations are obtained by the curvilinear version of complete pressure correction algorithm of Date (1996). For further details, see Ray (1999). In this method, since all the variables are stored at the same node, the cell face velocities (used to calculate the convective coefficients and the mass fluxes) are obtained by linear interpolation and the pressure gradients are expressed by central difference formula. This procedure normally leads to pressure checker boarding. However, the novel feature of this method is the introduction of the *smoothing* pressure correction in the pressure correction equation, which accounts for the residues of the momentum equations at the cell faces. The continuity equation is solved for the *total* pressure correction, which is the sum of the *smoothing* pressure correction and the *mass conserving* pressure correction. The former equals to the half of the difference between the nodal value of pressure and the cell averaged value of pressure, while the latter is used to correct the nodal values of pressure and velocities.

In the present problem as the forced convection situation is considered, the continuity and the momentum equations are first solved to obtain the flow field for different values of β_p to cover a wide range of Reynolds number ($30 \leqslant Re \leqslant 1100$). The energy equation is solved afterwards for different Prandtl numbers ($0.1 \leqslant Pr \leqslant 500$), using the converged velocity fields. These computations are carried out for six different twist ratios ($1.5 \leqslant Y \leqslant 10$).

3.2. Convergence criterion and CPU time requirement

The residues of the discretised continuity, and momentum equations at each control volumes are calculated to check the convergence of the velocity field. If $R^{\phi}_{i,j,k}$ is the residue of the ϕ conservation equation at a control volume corresponding to the index location, (i,j,k), then the L_2 norm is evaluated as $L_2 = \left(\sum_{i,j,k} R^{\phi^2}_{i,j,k}\right)^{1/2}$. The L_2 for all the governing equations are evaluated. Convergence is achieved, when these norms fall below 10^{-6}. It is also observed that further lowering of this criterion does not improve the results of average Reynolds number and friction factor. For the energy equation, the maximum change per iteration in the values of the temperature is monitored in the computational domain. The solution is accepted, when the maximum change in temperature falls below 10^{-5}.

Number of iterations required to achieve converged solution typically varies from 300 to 600, depending on the twist ratio and Reynolds number. It increases with the increase in Reynolds number and decrease in twist ratio. The solutions are obtained with under-relaxation parameters, $\alpha = 0.5$ and $\alpha_p = 0.1$. All the computations in the present study are carried out on DEC-ALPHA 2100 system at Indian Institute of Technology, Bombay. The typical CPU time required per 100 iterations of the fluid flow problem is approximately 1050 s. For the solution of energy equation, the typical CPU time requirement is approximately 270 s, for the same number of iterations.

4. Results and discussion

Dimensional analysis of the transport equation shows that the friction and heat transfer characteristics can be presented as

$$f = f(Re, Y, \delta/a), \tag{7}$$

$$Nu = Nu(Re, Y, Pr, \delta/a \text{ Boundary Conditions}). \tag{8}$$

However, in the present study, tape thickness is assumed to be negligible ($\delta/a = 0$). H_2 boundary condition is prescribed on the duct wall and the tape is assumed to be non-conducting (zero fin effect, as the tape makes only point contact after each $\pi/2$ rotation).

4.1. Reynolds number, friction factor and Nusselt number

From the converged solutions, the mean axial velocity is calculated as

$$\bar{u}_3 = \frac{1}{A_c} \int_{A_c} u_3 \, dA_3, \tag{9}$$

where A_c is the cross-sectional area at the corresponding axial location and dA_3 is the elemental area on the plane of constant ξ_3. From the mean axial velocity, the average Reynolds number, defined on the basis of the side of an empty square duct, is calculated at each axial station as

$$Re = \rho \bar{u}_3 a/\mu. \tag{10}$$

The values of Re at different axial stations are found to vary only in the fourth decimal place. The average friction factor, based on the hydraulic diameter of the empty tube is then calculated according to following relation

$$\Delta p = 4f\left(\frac{L}{a}\right)\cdot\frac{\rho\bar{u}_3^2}{2}, \tag{11}$$

which can be rearranged to read as

$$f = \beta_p a/2\rho\bar{u}_3^2. \tag{12}$$

Since $H2$ boundary condition (see Shah and London, 1978 for details) is used in the present problem, the wall temperature along the periphery of the duct at a particular cross-section is obtained from the converged solutions of the energy equation. The average wall temperature and the bulk temperature of the fluid at each axial location are then calculated as follows,

$$\bar{T}_w = \frac{1}{S_c}\int_{S_c} T_w\,ds, \tag{13}$$

$$T_b = \int_{A_c}\rho C_p u_3 T\,dA_3 \Big/ \int_{A_c}\rho C_p u_3\,dA_3, \tag{14}$$

where S_c is the total length along the periphery of the duct. From Eqs. (13) and (14), the cross-section averaged heat transfer coefficient, h_{x_3}, and the Nusselt number, Nu_{x_3} at each axial station, x_3, are calculated as

$$h_{x_3} = q_w/(\bar{T}_w - T_b), \tag{15}$$

$$Nu_{x_3} = h_{x_3}a/k. \tag{16}$$

Here also, the cross-sectional (or, local) average Nusselt number is defined on the basis of a, the hydraulic diameter of the empty square duct. The overall average (i.e., length or pitch averaged) heat transfer coefficient, $\bar{h}$, and the Nusselt number, $\overline{Nu}$ are then calculated as

$$\bar{h} = \frac{1}{2H}\int_0^{2H} h_{x_3}\,dx_3, \tag{17}$$

$$\overline{Nu} = \bar{h}a/k. \tag{18}$$

4.2. Variation of friction factor

The variations of friction factor with Reynolds number for different twist ratios are presented in Fig. 3. From the figure, it is observed that the friction factor increases with the decrease in twist ratio. The effect of twist ratio is also more prominent for higher Reynolds number. This is expected, since with the decrease in the twist ratio the strength of the secondary flow, generated by the tape, also increases. Under this condition, the fluid also travels a longer path through the duct (Manglik and Bergles, 1993a). The strength of the secondary flow, and hence, the flow resistance, also increases with the increase in the axial velocity of the fluid. As a result, the curves for different twist ratios, depart more for higher Reynolds number and asymptotically tend towards the curve for $Y = \infty$ for lower Reynolds number.

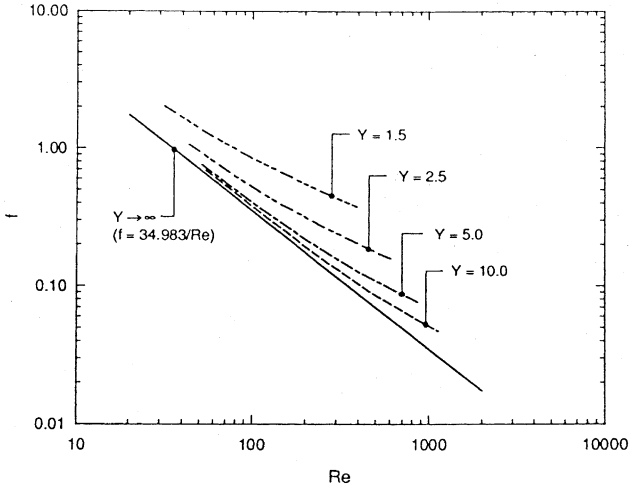

Fig. 3. Variation of f with Re.

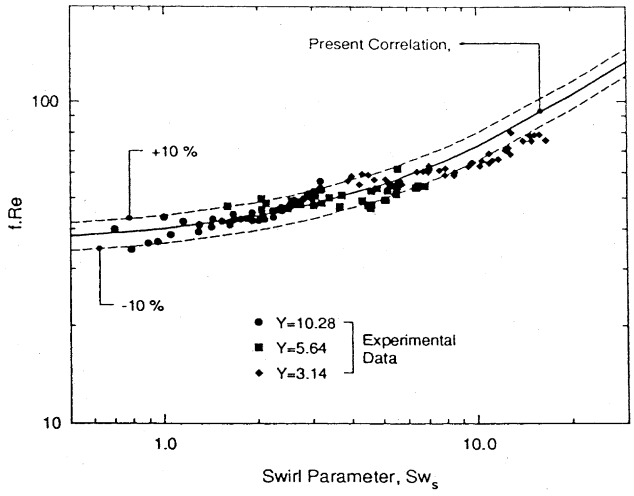

Fig. 4. Comparison of present correlation with experimental data.

4.3. The correlation for friction factor

When a straight tape ($Y = \infty$) is inserted in a square duct, the tape divides the duct into two equal rectangular halves. The friction factor for such rectangular ducts, with aspect ratio of 2, is obtained as $f\cdot Re = 34.983$ (based on the hydraulic diameter, a, (Shah and London, 1978)). It is also evident from Fig. 3 that $f\cdot Re$ should be represented by this value, either as $Re \to 0$, or, as $Y \to \infty$. Finally, however, based on the curve-fit to the present numerical data, the correlation of $f\cdot Re$ is obtained as [1]

$$f\cdot Re = 36[1 + 0.15\ Sw_s]^{1/1.3}, \tag{19}$$

where Sw_s is the notational swril parameter for the square duct and is given by

$$Sw_s = \left(\frac{Re}{Y}\right)^{3/4}\left[\frac{1+0.01Y^4}{Y^6}\right]^{1/4}. \tag{20}$$

Recently, Ray (1999) has performed an experimental study on pressure drop through a smooth square duct with twisted tape insert, using water as working fluid. The experimental data of Ray (1999) and the correlation of $f\cdot Re$ are plotted against Sw_s in Fig. 4. The comparison shows a reasonably good agreement (almost 90% of the data lie within ±10%) with Eq. (19).

4.4. Variation of Nusselt number

The variations of length averaged Nusselt number, $\overline{Nu}$, with Reynolds number, for $Y = 1.5, 2.5, 5$ and 10.0 and for different Prandtl numbers are presented in Figs. 5(a–d), respectively. The results show that with the decrease in twist ratio, the length averaged Nusselt number increases. This is expected, since, for twisted tape inserted ducts, swirl (the secondary

[1] Note, that this correlation cannot be applied as $Re \to 0$, as the limiting value is taken as 36.

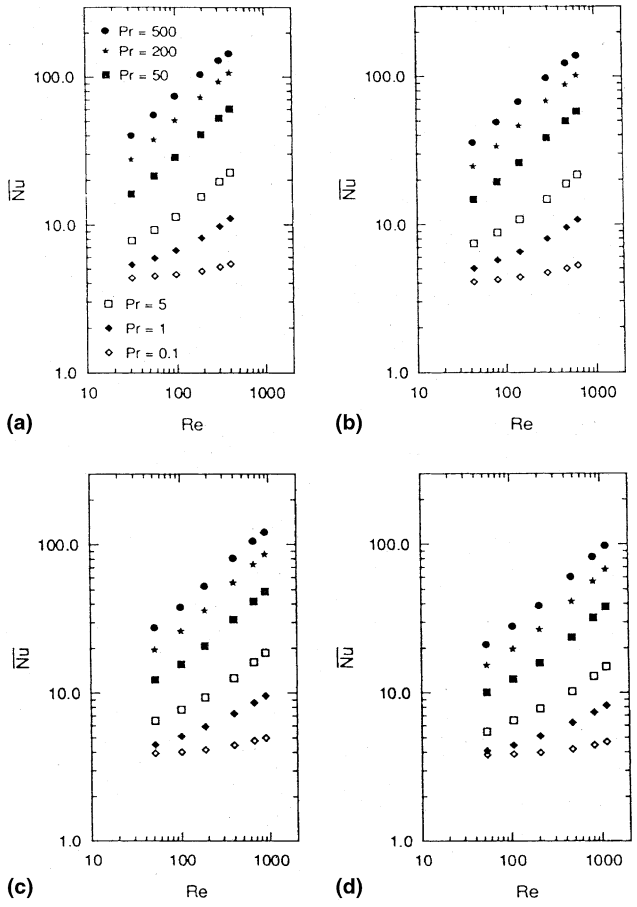

Fig. 5. Variation of $\overline{Nu}$ with Re: (a) $Y = 1.5$; (b) $Y = 2.5$; (c) $Y = 5$; (d) $Y = 10.0$.

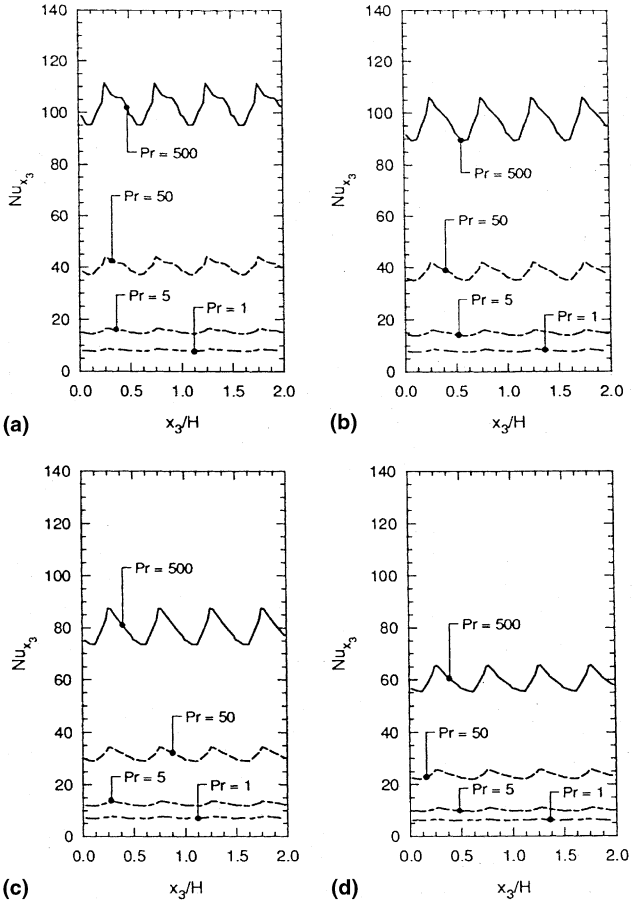

Fig. 6. Variation of Nu_{x_3} with x_3/H (effect of Pr): (a) $Y = 1.5$, $Re = 188.5$; (b) $Y = 2.5$, $Re = 283.07$; (c) $Y = 5$, $Re = 394.62$; (d) $Y = 10$, $Re = 473.04$.

motion) is additional mechanism for convective heat transfer and with the decrease in twist ratio, the strength of the secondary motion increases. The strength of the swirling motion also increases with the increase in the average axial velocity. As a result, the length averaged Nusselt number increases with Reynolds number. From these figures, it is also observed that the length averaged Nusselt number increases with Prandtl number. This is because the swirl generated transverse boundary layers becomes thinner with the increase in Prandtl number. The figure also clearly show that $\overline{Nu}$ tends to its value corresponding to $Y = \infty$ as $Re \to 0$.

The variations of local Nusselt number, Nu_{x_3} with axial distance, x_3 are presented in Figs. 6 and 7, where, the effect of Pr and Re are shown, respectively. From these figures, it is observed that the magnitude of variation increases with the increase in both Re and Pr. For lower values of Prandtl number, $(0.1 \leqslant Pr < 1)$, the axial variation in Nu_{x_3} is almost negligible. For higher Prandtl number, the maximum occurs at those axial location, where the tape is aligned with the diagonal of the duct (i.e., at θ's multiple of 45°). The same trend is observed for all the twist ratios. The figures also clearly indicate that for forced convection flow, the axial periodicity indeed occurs over a distance of $H/2$.

4.5. The correlation for Nusselt number

The Nusselt numbers for flow through rectangular ducts with $H2$ boundary conditions at all the four boundaries are available in Shah and London (1978). However, in the present problem, the tape surface is considered to be insulated and we are not aware of any data, which corresponds to this situation. The limiting case of twisted tape, with $Y = \infty$, however, can be analysed by variational method (see Ray, 1999 for details). This method yields $\overline{Nu}_\infty = 3.96$. This situation has also been numerically computed and the average predicted value is 3.958.

The length averaged Nusselt number, $\overline{Nu}$ is expected to be a function of Re, Pr and Y. Hong and Bergles (1976) have pointed out that the dimensionless group of numbers, that affect the Nusselt number for circular ducts with twisted tape inserts, can be clubbed into $Pr^{0.7}(Re/Y)^{1.25}$. However, for the present problem, it is observed that although the form of the correlation for square ducts remains the same as that for circular duct, the Prandtl number dependence is different from that of Hong and Bergles (1976). Finally, the correlation, based on the curve fit to the numerical data, is obtained as

$$\overline{Nu} = 3.96\left[1 + 1.6 \times 10^{-2} Pr^{1.05}\left(\frac{Re}{Y}\right)^{1.25}\right]^{1/2.6}. \tag{21}$$

The comparison of the above correlation with the raw Nusselt number data are plotted against the newly observed parameter, $Pr^{1.05}(Re/Y)^{1.25}$, in Fig. 8. The comparison shows reasonably good agreement (almost 90% of the data lie within ±10%) with Eq. (21).

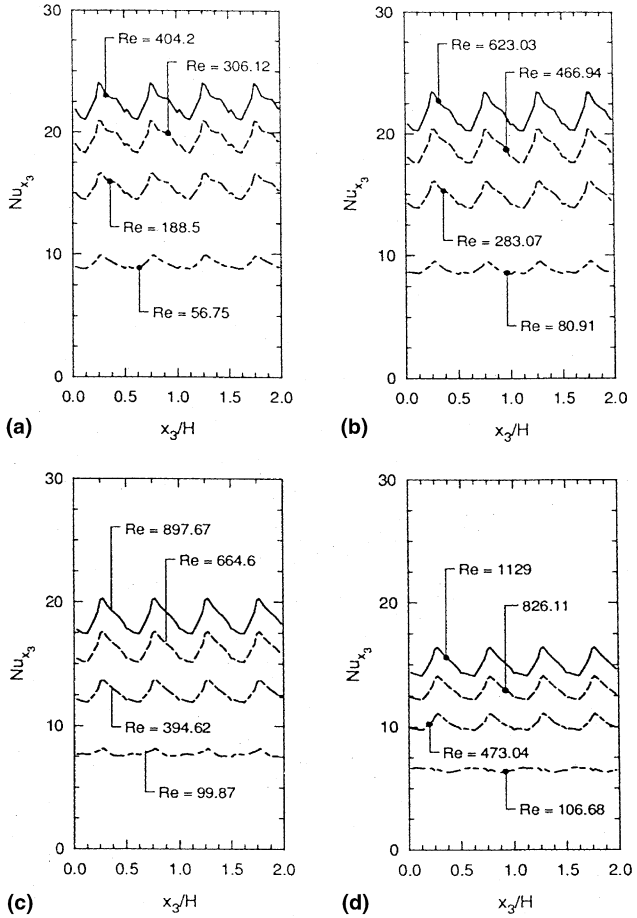

Fig. 7. Variation of Nu_{x_3} with x_3/H (effect of Re): (a) $Y = 1.5$; (b) $Y = 2.5$; (c) $Y = 5$; (d) $Y = 10$.

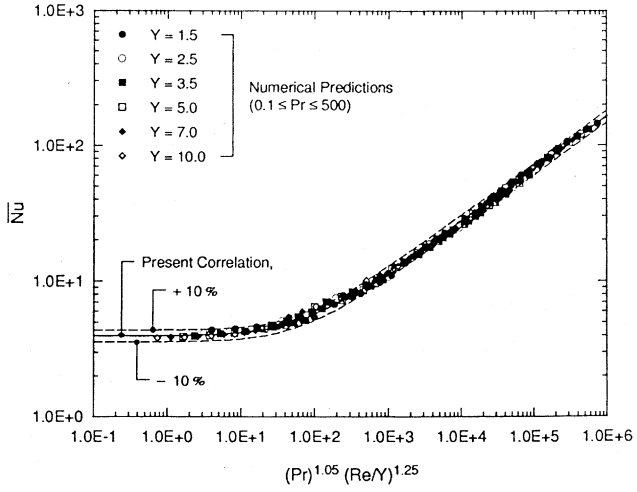

Fig. 8. Correlation of $\overline{Nu}$ with $(Pr)^{1.05}(Re/Y)^{1.25}$.

4.6. Presentation of the flow structure

4.6.1. Secondary flow

The secondary velocity vector at a cross-section can be obtained by vectorially summing the u_1 and u_2 velocity components. While plotting, the vectors are also normalised with respect to the average axial velocity. The secondary velocity distribution at $\theta = 45°$ (i.e., $x_3 = H/4$) for $Y = 1.5$, is presented in Figs. 9(a) and (b), respectively, for $Re = 189$ and 404. The figures clearly indicate the existence of strong swirling motion within the duct. The magnitude of the secondary velocity at some locations is observed to be even higher than the average axial velocity. The figures are also similar in appearance, as the maximum normalised secondary velocity does not change appreciably [2] with the increase in Re. The secondary velocity distributions are also presented in Figs. 10(a) and (b) for $Y = 2.5$ (for $Re = 283$) and 5 (for $Re = 395$), respectively. From these figures it is observed that as the twist ratio increases, the strength of the secondary flow considerably decreases. [3]

4.6.2. Axial velocity distribution

The axial velocity contours for $Y = 1.5$ are presented in Figs. 11(a) and (b) for $Re = 189$ and 404, respectively. Figures show that with the increase in Reynolds number, the fluid experiences more centrifugal force and the location of the maximum axial velocity [4] shifts towards the tip of the tape in the direction of rotation. The velocity gradient near the tape, particularly the portion which drives the flow, is also higher than that near the duct surface. It is also observed that with the increase in Reynolds number, the change in velocity near the tape surface occurs more rapidly,

4.6.3. Isotherms

The isotherms [i.e., $(T - \bar{T}_w)/(\bar{T}_w - T_b)$] for $Y = 1.5$ and $Re = 189$ are presented in Figs. 12(a) and (b) for $Pr = 1$, and 500, respectively. From these figures it is observed that with the increase in Prandtl number, the transverse thermal boundary layer thickness, generated by the secondary flow becomes thinner and larger temperature drop occurs near the wall. At very high Prandtl number, the temperature distribution shows almost a thermal boundary layer pattern near the duct surface.

5. Relative thermo-hydraulic performances of ducts with square and circular cross-sections

Usually, the pressure drop and heat transfer characteristics of flow in enhanced ducts are highly nonlinear. As such, it becomes almost impossible to make general statements about the superiority of one technique over the other. Bergles et al. (1974a,b, 1981b), Webb and Eckert (1972), Webb (1981) and Webb and Bergles (1983), for example, have therefore introduced several criteria for the assessment of overall improvement in thermo-hydraulic performance under specific conditions. However, in the present study, the attention is restricted to the single tube configuration, rather than an actual heat exchanger containing these tubes.

The study in this paper is concerned with the assessment of relative performances of four duct geometries under laminar flow conditions:

1. An empty circular duct,
2. An empty duct with square cross-section,
3. A duct of circular cross-section with twisted tape inserts,
4. A duct of square cross-section with twisted tape inserts.

It is known and will be shortly clear that a circular tube with a twisted tape insert provides superior thermo-hydraulic per-

[2] The maximum normalised secondary velocity is 1.089 for $Re = 188.5$ and 1.028 for $Re = 404.2$.

[3] The maximum normalised secondary velocity is 0.636 for $Y = 2.5$, as compared to 0.35 for $Y = 5$.

[4] The maximum axial velocities are 1.947 and 1.865 for $Re = 189$ and 404, respectively.

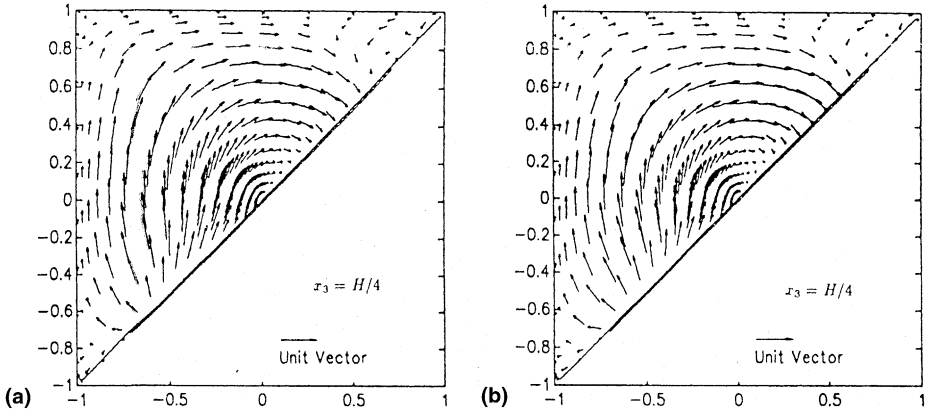

Fig. 9. Secondary velocities for $Y = 1.5$: (a) $Re = 189$; (b) $Re = 404$.

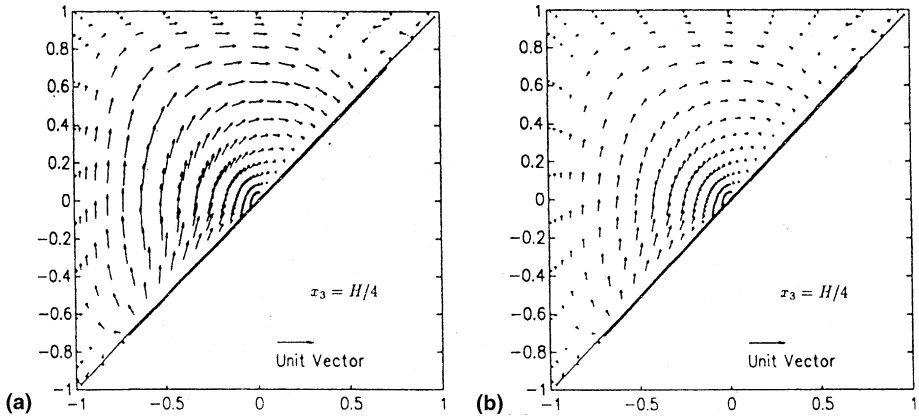

Fig. 10. Secondary velocities for: (a) $Y = 2.5$ ($Re = 283$); (b) $Y = 5$ ($Re = 395$).

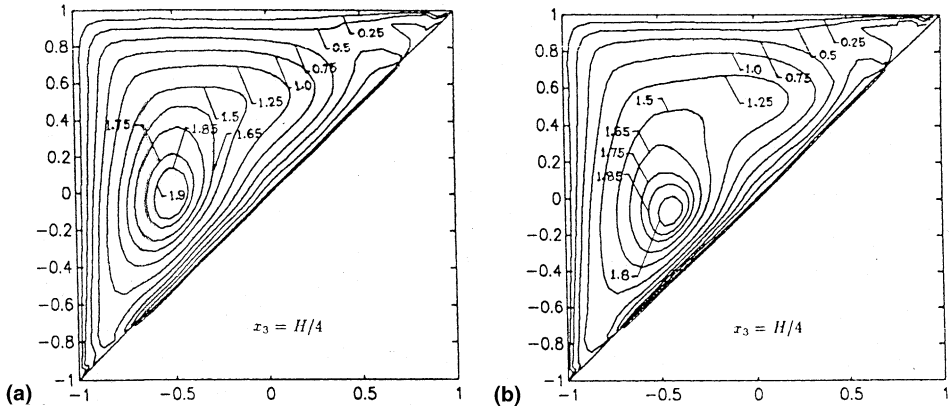

Fig. 11. Axial velocity contours for $Y = 1.5$: (a) $Re = 189$; (b) $Re = 404$.

formance as compared to an empty tube under laminar flow conditions, particularly when the Prandtl number is high. The main purpose of this study is to examine the performance of a square duct with that of a circular duct when both ducts are inserted with a twisted tape of same twist ratio. However, for the sake of completeness, the following comparisons of relative thermo-hydraulic performances are also provided.

1. Empty circular duct with circular duct containing a twisted tape,
2. Empty square duct with square duct with twisted tape inserts,
3. Empty circular duct with square duct fitted with a twisted tape,
4. Circular and square duct, both containing twisted tapes of same twist ratio.

5.1. Performance evaluation criteria

5.1.1. Definition

Bergles et al. (1974a) have introduced seven performance evaluation criteria (PEC) in each of which, there is one

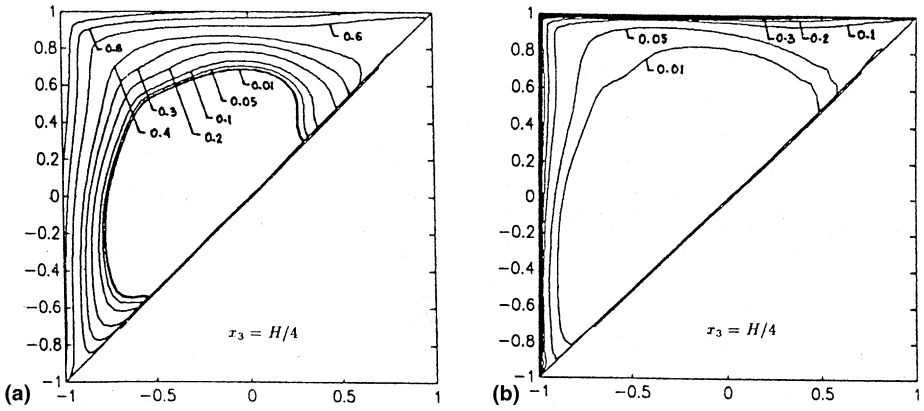

Fig. 12. Isotherms for $Y = 1.5$, $Re = 189$: (a) $Pr = 1$; (b) $Pr = 500$.

Table 3
Objective functions and fixed parameters for different PECs

PEC	Objective	Fixed parameter 1	Fixed parameter 2
R_1	Increased heat transfer	Geometry	Mass flow rate
R_2	Increased heat transfer	Geometry	Pressure drop
R_3	Increased heat transfer	Geometry	Pumping power
R_4	Reduced pumping power	Geometry	Heat duty
R_5	Reduced size	Pumping power	Heat duty
R_6	Reduced size	Pressure drop	Heat duty
R_7	Reduced size	Mass flow Rate	Heat duty

objective function and two fixed parameters (see Table 3). In all the evaluations, the mass flow rate, $\dot{m}$, and the heat transfer rate (or, heat duty), $\dot{Q}$, for the square (denoted with suffix, s) and circular (denoted with suffix c) ducts are calculated as

$$\dot{m}_s = \rho a^2 V_s, \tag{22}$$

$$\dot{m}_c = \rho(\pi/4)D^2 V_c, \tag{23}$$

$$\dot{Q}_s = h_s 4aL_s(\Delta T)_s, \tag{24}$$

$$\dot{Q}_c = h_c \pi D L_c (\Delta T)_c. \tag{25}$$

All evaluations are carried out under the assumption of $(\Delta T)_s = (\Delta T)_c$. In the context of the present study, the term "basic geometry fixed" requires careful definition. It is assumed that the length (L) and the twist ratio (Y) for the two ducts are identical. Further comparisons can be made such that either the hydraulic diameters are equal, or, the cross-sectional areas are equal. In the present study, whenever the performance of a circular duct is compared with its square counterpart, each parameter is evaluated under both of these assumptions. Thus,

$$R_i(1) \text{ implies} \quad D = a \text{ or } \quad a/D = 1, \tag{26}$$

$$R_i(2) \text{ implies} \quad (\pi/4)D^2 = a^2 \text{ or } \quad a/D = \sqrt{\pi/4}. \tag{27}$$

Finally, as will become apparent shortly, evaluation of PECs requires knowledge of friction factor, f and Nusselt number, Nu, for each duct. For empty circular duct f and Nu are given by $16/Re$ and 4.36, respectively, whereas, they are given as $14.227/Re$ and 3.091, respectively, for empty square duct (Shah and London, 1978). The friction factor (Manglik and Bergles, 1993a) and Nusselt number (Hong and Bergles, 1976) for circular duct, with twisted tape insert are evaluated from

$$f_c = \frac{42.232}{Re_c}\left[\frac{\pi^2 + 4Y^2}{4Y^2}\right][1 + 10^{-6} Sw_c^{2.55}]^{1/6}, \tag{28}$$

where Sw_c is the appropriate swirl parameter for circular duct, given as

$$Sw_c = 0.5\frac{Re_c\sqrt{4Y^2 + \pi^2}}{Y^{3/2}} \tag{29}$$

and

$$Nu_c = 5.172\left[1 + 0.005484(Pr)^{0.7}\left(\frac{Re_c}{Y}\right)^{1.25}\right]^{0.5}. \tag{30}$$

These correlations are obtained for non-conducting tapes by assuming the tape thickness to be zero. The Nusselt number correlations are obtained for axially and peripherally constant wall heat flux condition.

5.1.2. Expressions for PECs

In this paper, the PECs are evaluated assuming circular duct as the "original" (un-augmented) geometry and square duct as enhanced configuration. The operating constraints and the expressions of different PECs are listed in Table 4. The derivation of these expressions are fairly straight forward (Ray, 1999). In general, Re_s is specified, and Re_c is obtained from the operating constraint, either directly (as in the case of R_1 and R_7) or, iteratively (as in case of others).

5.2. Results and discussion

In the present study, four different fluids are considered. These are – air ($Pr = 0.7$), water ($Pr = 5$), moderately high Prandtl number fluid ($Pr = 50$) and fluid with very high Prandtl number ($Pr = 500$). For each fluid, four twist ratios are considered ($Y = 1.5, 2.5, 5$, and 10) and the Reynolds number is varied from 10 to 1000.

Table 4
Constraints and expressions for different PECs

PEC	Operating constraint	Expression of PEC
R_1	$Re_c/Re_s = (4/\pi)(a/D)$	$(4/\pi)(L_s/L_c)(Nu_s/Nu_c)$
R_2	$Re_c/Re_s = [(D/a)^3(L_s/L_c)(f_s/f_c)]^{1/2}$	$(4/\pi)(L_s/L_c)(Nu_s/Nu_c)$
R_3	$Re_c/Re_s = [(4/\pi)(D/a)^2(L_s/L_c)(f_s/f_c)]^{1/3}$	$(4/\pi)(L_s/L_c)(Nu_s/Nu_c)$
R_4	$Nu_c = (4/\pi)(L_s/L_c)Nu_s$	$(4/\pi)(D/a)^2(L_s/L_c)(f_sRe_s^3/f_cRe_c^3)$
R_5	$Re_c/Re_s = [(D/a)^2(Nu_c/Nu_s)(f_s/f_c)]^{1/3}$	$(a/D)^3(f_cRe_c^3/f_sRe_s^3)$ or $(a/D)(Nu_c/Nu_s)$
R_6	$Re_cRe_s = [(\pi/4)(D/a)^3(Nu_c/Nu_s)(f_s/f_c)]^{1/2}$	$(4/\pi)(a/D)^4(f_cRe_c^2/f_sRe_s^2)$ or $(a/D)(Nu_c/Nu_s)$
R_7	$Re_c/Re_s = (4/\pi)(a/D)$	$(4/\pi)(a/D)(1/R_1)$

5.2.1. Comparison of an empty circular tube and a circular tube containing a twisted tape

In this case, the operating constraint for PEC-I is given by, $Re_o = Re_a$. [5] Also, the value of R_1 is obtained as, $R_1 = Nu_a/Nu_o$. Therefore, it is given by

$$R_1 = 1.186\left[1 + 0.005484(Pr)^{0.7}\left(\frac{Re_c}{Y}\right)^{1.25}\right]^{0.5}. \quad (31)$$

Similarly, the operating constraints for PEC-II and III can be obtained as $Re_o/Re_a = (f_a/f_o)^{1/3}$, $Re_o/Re_a = (f_a/f_o)^{1/3}$, respectively. However, for a particular value of Re_a, irrespective of Re_o as obtained by satisfying the constraint, the values of R_2 and R_3 are same as R_1. It is interesting to note that R_1 is always greater than unity (which implies improved performance) irrespective of Re, Pr and Y.

The constraint for PEC-IV is given by $Nu_o = Nu_a$. Unfortunately, since Nu_a is always greater than Nu_o, this constraint can never be satisfied and hence no comparison is possible. The constraints for PEC-V and VI can be obtained as $Re_o/Re_a = [(Nu_o/Nu_a)f_a/f_o]^{1/3}$, $Re_o/Re_a = [(Nu_o/Nu_a)f_a/f_o]^{1/2}$, respectively. For these cases R_5 and R_6 can be shown to be equal to Nu_o/Nu_a. Therefore, they are simply the inverse of R_1 and are always less than unity (implying improved performance). As a result, these values are not presented here.

5.2.2. Comparison of an empty square tube and a square tube containing a twisted tape

The analysis for this case is exactly same as that carried our for the earlier case. The expressions for the constraints and R_i's (in terms of f and Nu) are also same. Here also, $R_1 = R_2 = R_3$ and $R_5 = R_6$, with R_5 being inverse of R_1. The expression for R_1 is, however, different from Eq. (31) and is given by

$$R_1 = 1.281\left[1 + 1.6 \times 10^{-2}Pr^{1.05}\left(\frac{Re_s}{Y}\right)^{1.25}\right]^{1/2.6}. \quad (32)$$

The above equation indicated that here also, R_1 is always greater than unity (and hence, $R_5 < 1$).

5.2.3. Comparison of an empty circular tube and a square tube containing a twisted tape

In this comparison, since Nu_o is independent of Re, Pr and Y, the values of R_1, R_2 and R_3 are equal. R_1, for example, is given by

$$R_1 = 1.156\left[1 + 1.6 \times 10^{-2}Pr^{1.05}\left(\frac{Re_s}{Y}\right)^{1.25}\right]^{1/2.6}. \quad (33)$$

[5] Here, suffix "o" and "a" denote the "original" and "augmented" configuration.

Here also, R_1 is always greater than unity, which implies that a square duct containing a twisted tape will perform better than an empty circular tube for any fluid, irrespective of Re and Y.

The expression for R_5 (or, R_6) is given in Table 4. Therefore, for Case-I (i.e., $a/D = 1$), R_5 is obtained as

$$R_5 = \frac{1.101}{\left[1 + 1.6 \times 10^{-2}Pr^{1.05}(Re_s/Y)^{1.25}\right]^{1/2.6}}. \quad (34)$$

Similar expression for Case-II (i.e., $a/D = \sqrt{\pi/4}$) is given by

$$R_5 = \frac{0.976}{\left[1 + 1.6 \times 10^{-2}Pr^{1.05}(Re_s/Y)^{1.25}\right]^{1/2.6}}. \quad (35)$$

It is obvious from Eqs. (34) and (35) that for Case-II, R_5 is always less than unity. However, for Case-I, a threshold

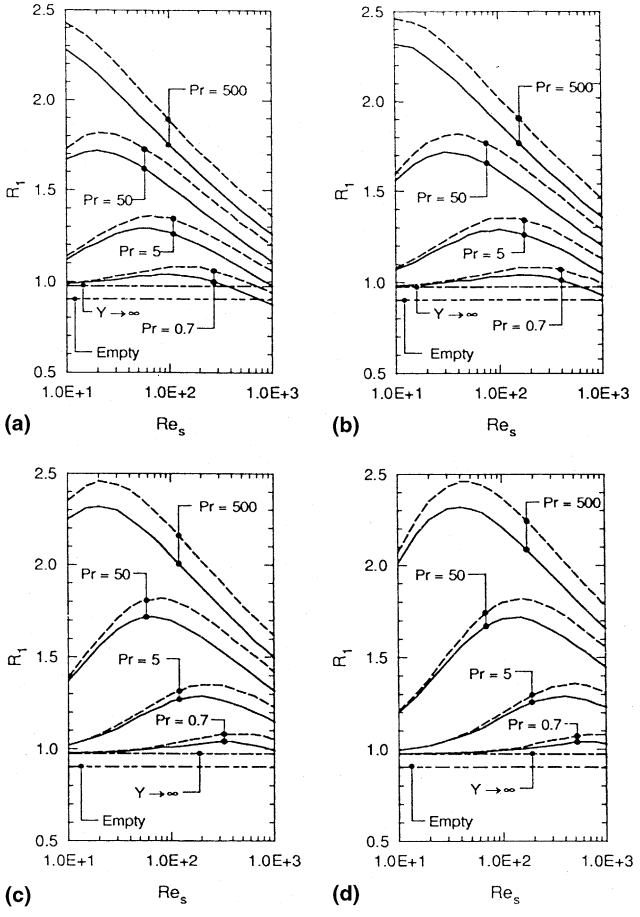

Fig. 13. Variation of R_1 with Re_s for different Pr and Y: (a) $Y = 1.5$; (b) $Y = 2.5$; (c) $Y = 5$; (d) $Y = 10$.

Reynolds number is obtained for each fluid, above which, better thermo-hydraulic performance is achieved with square duct. The threshold value of Re again depends on the twist ratio. This value can be obtained by setting $R_5 = 1$ and the corresponding expression is given by

$$Re_{\text{th}} = \left[\frac{17.767}{Pr^{1.05}} Y\right]^{1/1.25}. \tag{36}$$

Obviously, Re_{th} decreases with the decrease in Y and increase in Pr. For example, when tape with a twist ratio of 10 is inserted into a square duct, Re_{th} is obtained as 134.84 and 25.86, respectively, for air ($Pr = 0.7$) and water ($Pr = 5$).

5.2.4. Comparison of circular and square tubes, both containing a twisted tape

The variations of R_1 to R_6 for this case are presented in Figs. 13–18. In all the figures, $R_i(1)$ are shown by solid lines and $R_i(2)$ by dotted lines. Figures clearly show that the thermo-hydraulic performance of square duct is better over a wide range of operating parameters. Irrespective of Re and Y, the performance of square duct improves with the increase in Pr for both the cases. It is also evident that Case-II shows better performance than Case-I, when parameter R_1 is considered as design criterion. However, if R_2 to R_5 are selected as design criteria, Case-I performs better than Case-II. For R_6, there are threshold values of Re_s for each combination of Pr and Y, below which, the performance of Case-I is better than Case-II.

Limiting cases. In Figs. 13–18, the comparison for two limiting cases are also presented. One, in which, the tubes are fitted with straight tapes ($Y \to \infty$) and the other, in which, the tubes are empty. For straight tape case, the limiting Nu for square and circular ducts are given by 3.96 and 5.172, respectively [see Eqs. (21) and (30)]. Therefore, the values of R_1 to R_3 for both the cases are obtained as 0.975. Similarly, R_5 and R_6 are obtained as 1.306 for case-I and 1.157 for case-II. Nusselt numbers for empty square and circular ducts are given by 3.091 and 4.36, respectively (Shah and London, 1978). Thus, R_1 to R_3 for empty tube is obtained as 0.903 for both cases, whereas, R_5 and R_6 can be evaluated as 1.41 for case-I and 1.25 for case-II.

Increase in heat transfer (R_1, R_2 and R_3). Here $R_i > 1$ indicates improved performance. From Fig. 13, it is observed that the thermo-hydraulic performance of square duct can increase up to 250% for very high Prandtl number fluids. For such fluids, when the twist ratio is small (say, 1.5 or 2.5), the performance parameter R_1 continuously decreases with Re_s. The optimal Re_s again increases with the increase in Y. For all other fluids, R_1 always shows a maxima, irrespective of Y, the corresponding Re_s, where maxima occurs, increases with the increase in Y. It is also interesting to note that except for air, the square duct always performs better than circular duct ($R_1 \geqslant 1$), irrespective of Re_s and Y. However, for air, although R_1 lies between 0.9 and 1.1, a range of Re_s is observed, where R_1 is greater than unity.

The behaviour of parameters R_2 and R_3, as observed in Figs. 14 and 15, respectively, are similar to that of R_1. However, the peak values differ considerably. For example, if R_2 is chosen as design criterion and very high Prandtl number fluid ($Pr = 500$)

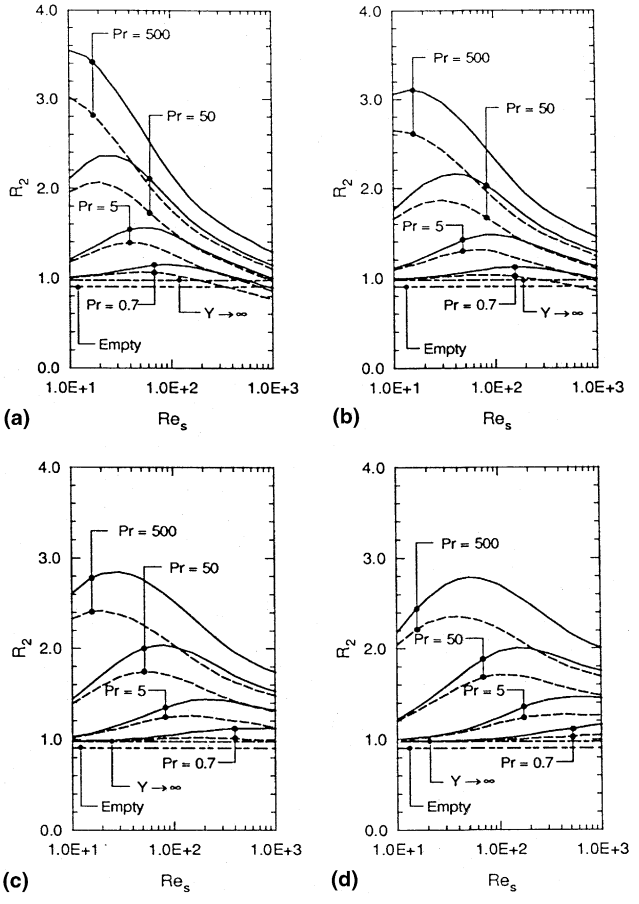

Fig. 14. Variation of R_2 with Re_s for different Pr and Y: (a) $Y = 1.5$; (b) $Y = 2.5$; (c) $Y = 5$; (d) $Y = 10$.

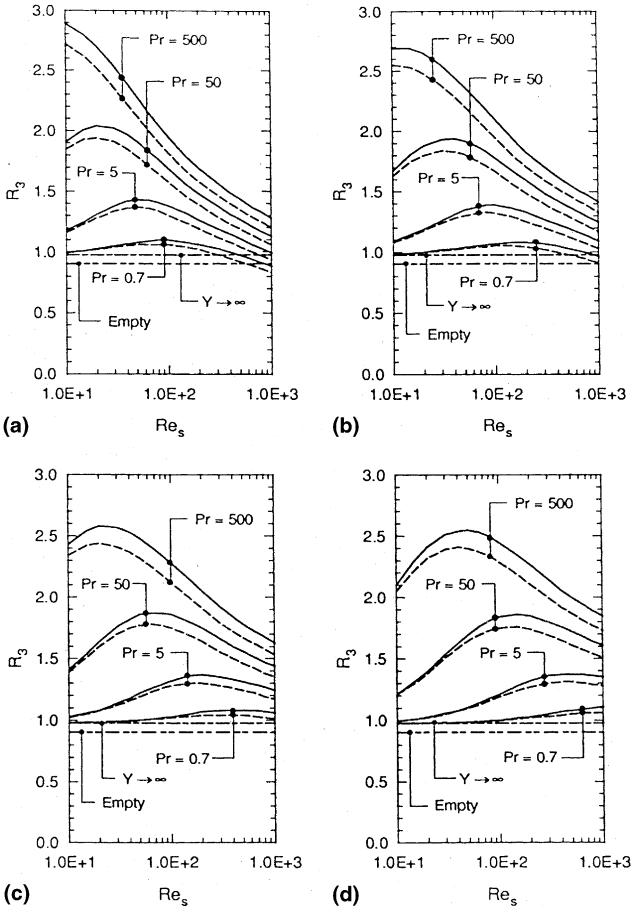

Fig. 15. Variation of R_3 with Re_s for different Pr and Y: (a) $Y = 1.5$; (b) $Y = 2.5$; (c) $Y = 5$; (d) $Y = 10$.

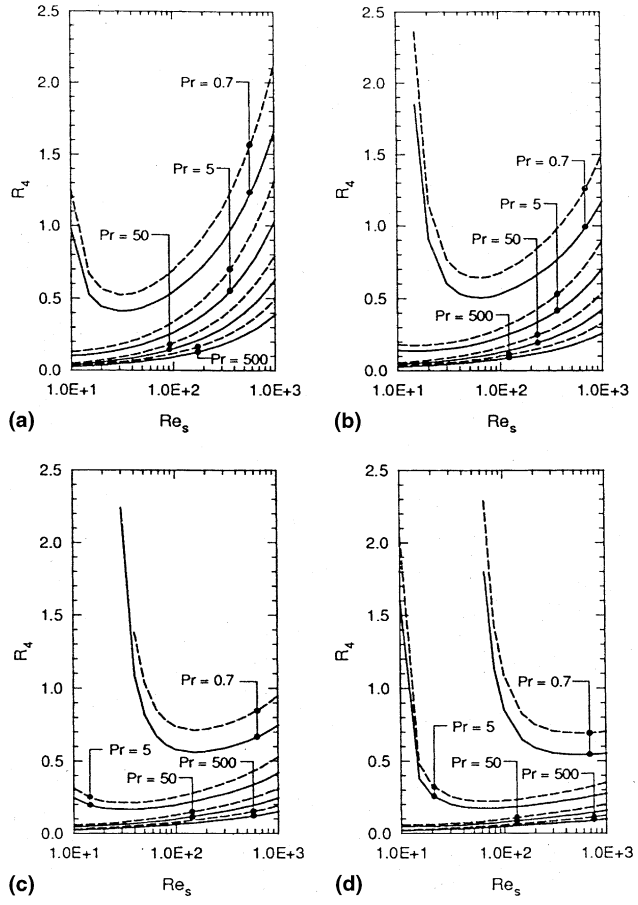

Fig. 16. Variation of R_4 with Re_s for different Pr and Y: (a) $Y = 1.5$; (b) $Y = 2.5$; (c) $Y = 5$; (d) $Y = 10$.

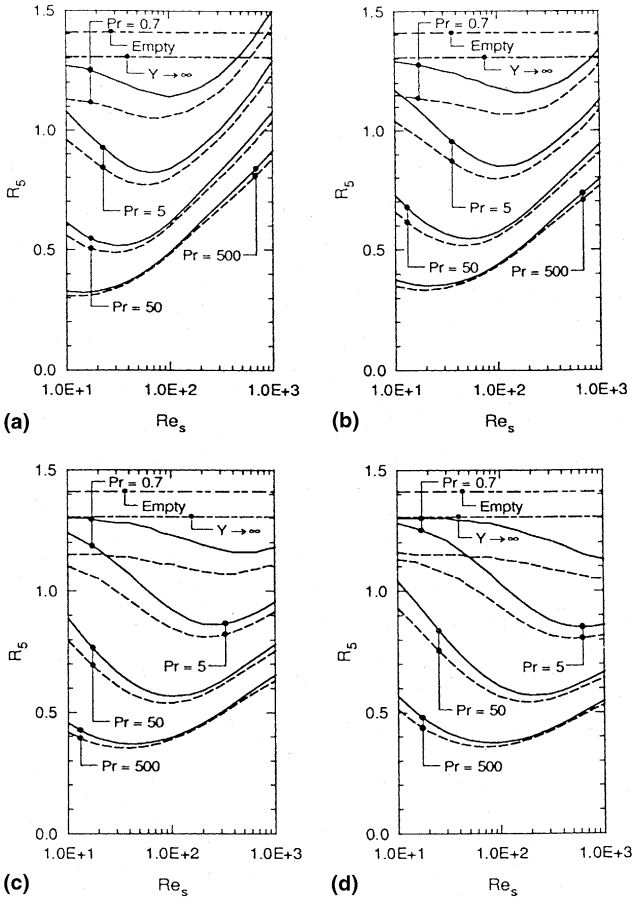

Fig. 17. Variation of R_5 with Re_s for different Pr and Y: (a) $Y = 1.5$; (b) $Y = 2.5$; (c) $Y = 5$; (d) $Y = 10$.

is used, around 350% improvement in the performance is achieved with square tubes for $Y = 1.5$. Similarly, under the same circumstances, with R_3 as design criterion, around 290% improvement is observed. It is also observed that the maximum value of R_2 and R_3 falls considerably with the increase in Y, particularly for fluids with higher Prandtl number.

Reduction in pumping power (R_4). *Here, $R_i < 1$ indicates improved performance*. The variation of R_4 with Re_s is presented in Fig. 16. It is observed from the figure that square ducts provide significant improvement in thermo-hydraulic performance even when air is used as working fluid. As expected, this advantage is achieved over range of operating Reynolds number, which considerably depends on twist ratio. At $Pr = 500$, the maximum reduction in pumping power is found to be 95%. Figure also shows that below a threshold Re_s, no comparison is possible as the operating constraint is not satisfied.

Reduction in heat exchanger size (R_5 *and* R_6). *Here, $R_i < 1$ indicates improved performance*. Figs. 17 and 18 show that if R_5 or R_6 is chosen as design criterion, no improvement can be achieved with square duct, if air is used as working fluid. Even for water, better performance is observed only within a range of Re_s for lower values of $Y(Y = 1.5$ and $2.5)$ and above a critical value of Re_s for higher values of $Y(Y = 5$ and $10)$. The values of critical Re_s depend considerably on Y. For all the fluids, an optimal Reynolds number is observed, where R_5 (and R_6) assumes a minimum value. The value of optimal Re_s again depends on Pr and Y and increases with the increase in Y, but decreases with the increase in Pr (an observation, similar to those observed for R_1 to R_3). However, when moderately high or very high Prandtl number fluid is used, square tubes show improved thermo-hydraulic performance, almost irrespective of Re_s and Y. For $Pr = 500$, the maximum reduction in exchanger surface area is observed to be 80%.

6. Conclusions

The following conclusions can be drawn from present study:

1. For a fixed Reynolds number, the friction factor increases with the decrease in twist ratio. The correlation for friction factor is given by Eq. (19), which compares within 10% with the experimental data for $100 \leqslant Re \leqslant 1100$ and $3.14 \leqslant Y \leqslant 10.28$.
2. The pitch-averaged Nusselt number, $\overline{Nu}$ increases with the increase in Reynolds number and Prandtl number and with the decrease in twist ratio. The correlation for $\overline{Nu}$ is given by Eq. (21).
3. When an empty circular or square duct is compared with the same duct containing a twisted tape, the thermo-hydraulic performance of the latter ducts is better for all Re, Pr and Y.
4. Increase in heat transfer of square tubes is considerably higher (up to a maximum of 350%) than the circular tubes, both fitted with tapes of same twist ratio, for fluids with higher Prandtl number, irrespective of Re_s and Y. Similarly, a maximum of 80% reduction in surface area is estimated.

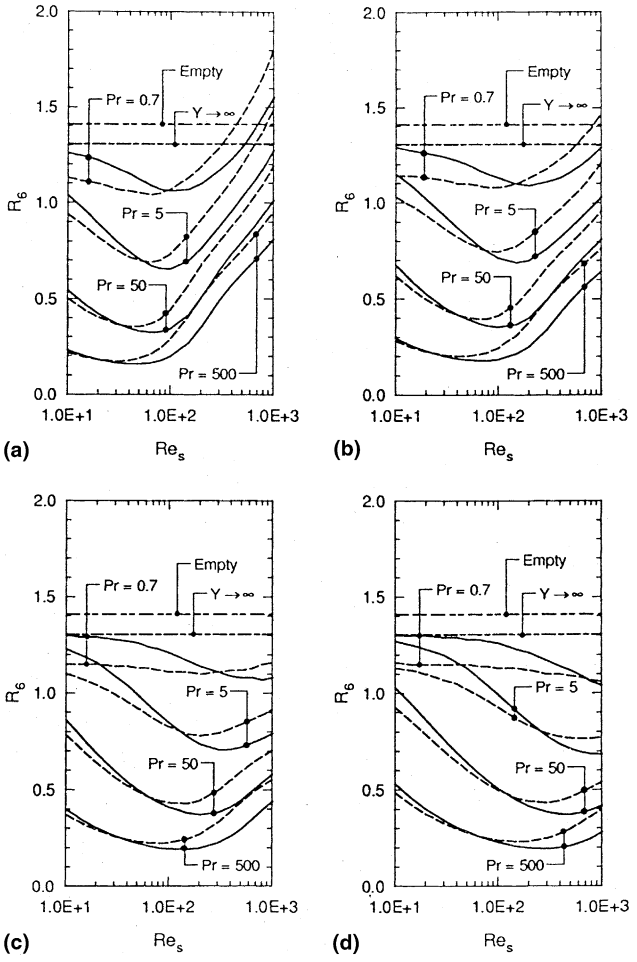

Fig. 18. Variation of R_6 with Re_s for different Pr and Y: (a) $Y = 1.5$; (b) $Y = 2.5$; (c) $Y = 5$; (d) $Y = 10$.

Alternatively, a maximum reduction in pumping power is estimated at 95%.

Acknowledgements

One of us, Dr. Subhashis Ray, would like to thank the authorities of Jadavpur University, for granting leave to carry out this research work.

References

Bergles, A.E., 1969. Survey and evaluation of techniques to augment convective heat and mass transfer. Prog. Heat Mass Transfer 1, 331–424.

Bergles, A.E., 1973. Recent developments in convective heat transfer augmentation. Appl. Mech. Rev. 26, 675–682.

Bergles, A.E., 1981a. Principles of heat transfer augmentaion I: Single phase heat transfer. In: Kakac, S., Bergles, A.E., Mayinger, F. (Eds.), Heat Exchangers: Thermal–Hydraulic Fundamentals and Design. Hemisphere Publishing Corporation, Washington, DC, pp. 819–842.

Bergles, A.E., 1981b. Applications of heat transfer augmentation. In: Kakac, S., Bergles, A.E., Mayinger, F. (Eds.), Heat Exchangers: Thermal–Hydraulic Fundamentals and Design. Hemisphere Publishing Corporation, Washinton, DC, pp. 883–911.

Bergles, A.E., Joshi, S.D., 1983. Augmentation techniques for low reynolds number in-tube flow. In: Kakac, S., Shah, R.K., Bergles, A.E. (Eds.), Low Reynolds Number Flow Heat Exchangers. Hemisphere Publishing Corporation, Washington, DC, pp. 695–720.

Bergles, A.E., 1985. Techniques to augment heat transfer. In: Rohsenow et al., W.M. (Eds.), Handbook of Heat Transfer Applications, second ed. McGraw Hill, New York.

Bhadsavle, V.S., 1994. Pressure drop characteristics of laminar and turbulent flow through a square duct fitted with full length twisted tapes. B.Tech. Project, Indian Institute of Technology, Bombay, India.

Bergles, A.E., Bunn, R.L., Junkhan, G.H., 1974a. Extended performance evaluation criteria for enhanced heat transfer surfaces. Lett. Heat Mass Transfer 1, 113–120.

Bergles, A.E., Blumenkrantz, A.R., Taborek, J. 1974b. Preformance evaluation criterion for enhanced heat transfer surfaces. In: Proceedings of the Fifth International Heat Mass Transfer Conference, Tokyo, vol. 2, pp. 239–243.

Date, A.W., 1996. A complete pressure correction algorithm for solution of incompressible Navier-Stokes equations on non-staggered grid. Numer. Heat Transfer, Part B 29, 441–458.

Hong, S.W., Bergles, A.E., 1976. Augmentation of laminar flow and heat transfer in tubes by means of twisted tape inserts. ASME., J. Heat Transfer 98, 251–256.

Manglik, R.M., Bergles, A.E., 1993a. Heat transfer and pressure drop correlations for twisted-tape inserts in isothermal tubes: Part I – laminar flows. ASME., J. Heat Transfer 115, 881–889.

Manglik, R.M., Bergles, A.E., 1993b. Heat transfer and pressure drop correlations for twisted-tape inserts in isothermal tubes: Part II – transition and turbulent flows. ASME., J. Heat Transfer 115, 890–896.

Mano, Y., Funahashi, N., Kobayashi, S., Kobayashi, M., Mori, Y., Ohhori, K., Nikai, I., Akane, M., Fuji, A., Kaneta, T., Urabe, S., 1986. Development of high temperature plate-fin heat exchanger for phosphoric acid fuel cell power system High Temperature Heat Exchangers. Hemisphere Publishing Corporation, Washington, DC, pp. 421–432.

Patankar, S.V., Liu, C.H., Sparrow, E.M., 1977. Fully developed flow and heat transfer in ducts having streamwise-periodic variations of cross-sectional area. ASME., J. Heat Transfer 99, 180–186.

Ray, S., 1999. Pressure drop and heat transfer characteristics of flow through square duct with twisted insert. Ph.D. Thesis, Indian Institute of Technology, Bombay, India.

Shah, R.K., London, A.L., 1978. Laminar flow forced convection in ducts Supplment 1, Advanced Heat Transfer. Academic Press, New York.

Sorenson, R.L., 1980. A computer program to generate a two-dimensional grid about an airfoil and other shapes by the use of Poisson's equation. NASA TM-81198.

Webb, R.L., 1981. Performance evaluation criteria for use of enhanced heat transfer surface in heat exchanger design. Int. J. Heat Transfer 24, 715–726.

Webb, R.L., 1987. Enhancement of single phase heat transfer. In: Kakac, S., Shah, R.K., Aung, W. (Eds.), Handbook of Single Phase Convective Heat Transfer. Wiley, New York, pp. 17.1–17.62.

Webb, R.L., Bergles, A.E., 1983. Performance evaluation criteria for selection of heat transfer surface geometries used in low reynolds number heat exchangers. In: Kakac, S., Shah, R.K., Bergles, A.E. (Eds.), Low Reynolds Number Flow Heat Exchangers. Hemisphere Publishing Corporation, Washington, DC, pp. 735–742.

Webb, R.L., Eckert, E.R.G., 1972. Application of rough surfaces to heat exchanger design. Int. J. Heat Mass Transfer 15, 1647–1658.